

# Self-balancing robot: modeling and comparative analysis between PID and linear quadratic regulator

Lu Bin Lau, Nur Syazreen Ahmad, Patrick Goh

School of Electrical and Electronic Engineering, Universiti Sains Malaysia, Nibong Tebal, Malaysia

## Article Info

### Article history:

Received Oct 20, 2022

Revised Mar 19, 2023

Accepted Apr 4, 2023

### Keywords:

Linear quadratic regulator

Modeling

Proportional-integral-derivative

Robot

Self-balancing

## ABSTRACT

A two-wheeled self-balancing robot (TWSBR) is an underactuated system that is inherently nonlinear and unstable. While many control methods have been introduced to enhance the performance, there is no unique solution when it comes to hardware implementation as the robot's stability is highly dependent on accuracy of sensors and robustness of the electronic control systems. In this study, a TWSBR that is controlled by an embedded NI myRIO-1900 board with LabVIEW-based control scheme is developed. We compare the performance between proportional-integral-derivative (PID) and linear quadratic regulator (LQR) schemes which are designed based on the TWSBR's model that is constructed from Newtonian principles. A hybrid PID-LQR scheme is then proposed to compensate for the individual components' limitations. Experimental results demonstrate the PID is more effective at regulating the tilt angle of the robot in the presence of external disturbances, but it necessitates a higher velocity to sustain its equilibrium. The LQR on the other hand outperforms PID in terms of maximum initial tilt angle. By combining both schemes, significant improvements can be observed, such as an increase in maximum initial tilt angle and a reduction in settling time.

*This is an open access article under the [CC BY-SA](#) license.*



## Corresponding Author:

Nur Syazreen Ahmad

School of Electrical and Electronic Engineering, Universiti Sains Malaysia

14300 Nibong Tebal, Penang, Malaysia

Email: syazreen@usm.my

## 1. INTRODUCTION

The past few decades have seen a growing interest in autonomous mobile robots (AMRs) in both industries and academia due to rapid technological advancements and the extensive use of robotics particularly for reducing costs and enhancing productivity [1]-[4]. A two-wheeled self-balancing robot (TWSBR) is one type of AMRs that is underactuated and inherently unstable but has notable advantages of being able to move on a zero-radius curve, high tolerance to impulsive force, and small footprints to move in dangerous places. The Segway Personal Transporter and Ninebot scooters are examples of commercialized technologies that apply the same concept of a TWSBR. Apart from being an alternative mode of transportation that can take the place of an automobile for short commutes, they have also been demonstrated useful for populations with a range of functional disabilities [5]. Although the user safety cannot be totally guaranteed [6]-[8], these technologies are often equipped with multiple control systems to enhance their reliability in the event of failure in any one of them, which in turn results in a higher cost.

In academia, the TWSBR is often used as a research platform to verify advanced control algorithms as its behaviour is comparable to that of the classical inverted pendulum system. Its wheels are usually driven

by an electrico-mechanical system which can be either direct current (DC) motors or stepper motors [9]. The main control objective is to stabilize the robot by driving all the state variables, which are the robot's position, velocity, tilt angle and angular velocity, to approach their desired stable values in the shortest time possible. In the TWSBR development, speed encoders, an accelerometer and a gyroscope are typically required to measure these state variables [10]. Many techniques have been proposed to solve the problem in the literature, which can be categorized into linear and nonlinear control approaches [11]-[14]. Examples of the latter include sliding mode controls [15], fuzzy logic control [16], [17], artificial neural network [18], and deep learning [19]. Aside from that, the Gaussian process (GP) has also been employed to its capability to create flexible nonlinear nonparametric models [20]. Chen *et al.* [21] explained for instance, a control design based on a learned GP regression model is proposed to alleviate the effects from modeling errors.

While the aforementioned nonlinear control methods have been demonstrated to provide robustness against uncertainties, the resulting complexity will typically limit their applicability to low-cost embedded controllers. The linear control approaches on the other hand are relatively simpler in terms of their implementations on hardware. The most popular methods are proportional-integral-derivative (PID) [22]-[24] and linear quadratic regulator (LQR) schemes [25]. Nevertheless, a notable downside of the PID control algorithm for controlling the TWSBR is the difficulty of parameter tuning [26], [27]. Although there are many software tools available to aid the optimization of the PID parameters, the resulting control law may not be desirable for the TWSBR which can be easily driven to the instability region. In contrast, controlling the TWSBR via the LQR scheme is relatively more straightforward as its optimal parameters can be obtained by minimizing the cost function that can also preserve the closed-loop stability at the same time. However, utilization of this controller requires prior knowledge and skills in analysing the trade off between the control performance and power consumption.

Most of the aforementioned work focused on developing new control strategies that can be validated via simulations. In practice, the system is not only inherently nonlinear and unstable, but is prone to random noise and disturbances [28]. Plus, there is no unique solution when it comes to hardware implementation as the robot's stability is highly dependent on the robustness of the electronic control systems. In this study, a TWSBR that is controlled by an embedded NI myRIO-1900 board with LabVIEW-based control scheme is developed. We compare the performance between PID and LQR schemes which are designed based on the robot's model that is constructed from Newtonian principles. A hybrid PID-LQR scheme is then proposed to compensate for the individual components' limitations. Experimental results demonstrate the PID is more effective at regulating the tilt angle of the robot in the presence of external disturbances, but it necessitates a higher velocity to sustain its equilibrium. The LQR on the other hand outperforms PID in terms of maximum initial tilt angle. By combining both schemes, significant improvements can be observed, such as an increase in maximum initial tilt angle and a reduction in settling time.

## 2. METHOD

### 2.1. TWSBR design and modeling

The TWSBR built in this study is shown in Figure 1 which consists of an NI myRIO-1900 board, two brushed DC motors with encoders, an external gyroscope (i.e. PmodGyro) to improve the tilt angle estimation (explained further in section 2.3), a 12 V Li-Ion power supply, a printed circuit board (PCB) containing the motor driver and voltage regulators, the wheels and the chassis. Figure 1(a) illustrates the built TWSBR while, Figure 1(b) visualizes the connection between each unit. The control scheme is constructed via model-based design approach in LabVIEW which is also used as a user interface to display and log the data wirelessly during the experiment.

The robot can be modeled from first principles by taking into account the dynamics of the motors, robot chassis, and the forces on the wheels. The inputs to the TWSBR are the torques applied to the left and right wheels, which are assumed to be similar. Figure 2 illustrates the free body diagram of the TWSBR. The diagram for the robot's wheel is depicted in Figure 2(a) where  $T_w$  denotes the torque applied to it,  $\theta$  is the angular position,  $F_w$  is the force applied to the wheel by the chassis, and  $F_f$  is the friction force by the surface contact. With regard to the robot chassis which includes the NI-myRIO board, batteries, gyroscope and the printed circuit board, it acts similar to an inverted pendulum as illustrated in Figure 2(b) whose base is attached to the wheels.

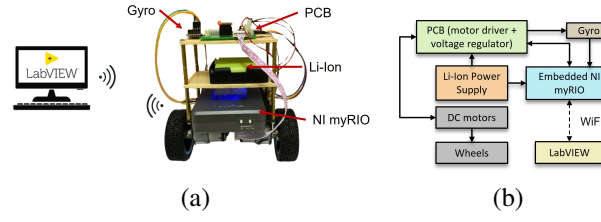


Figure 1. The TWSBR's prototype built in (a) this study and (b) its connection diagram

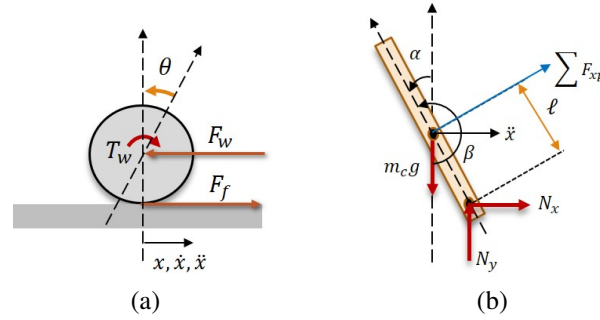


Figure 2. Free body diagrams of (a) the wheel and (b) the TWSBR's chassis

Let  $J_w$  be the moment of inertia of the wheel,  $r$  be its radius,  $m_w$  be mass of the wheel, and  $x$  be the horizontal position of the center of the wheel relative to a defined origin. Using Newton's law of motion, the sum of forces in the horizontal  $x$ -direction can be written as (1):

$$m_w \ddot{x} = F_f - F_w \quad (1)$$

for each wheel. Assuming there are no tire deformation and rolling resistance, the sum of torques is given by (2):

$$J_w \ddot{\theta} = T_w - F_f r \quad (2)$$

for each wheel. From the DC motor dynamics, the torque relates to the input voltage as  $T_w = (k_m/R)V_{in} - (k_m k_e/R)\dot{\theta}$ , where  $R$  is the electrical resistance of the motor, and  $V_{in}$  is the applied voltage, and  $k_m$  and  $k_e$  are torque and back EMF constants respectively. Substituting this expression into (2), we will get (3).

$$F_f = (k_m/Rr)V_{in} - (k_m k_e/Rr^2)\dot{x} - (J_w/r^2)\ddot{x}. \quad (3)$$

Replacing  $F_f$  in (1) with this expression gives (4).

$$F_w = (k_m/Rr)V_{in} - (k_m k_e/Rr^2)\dot{x} - (m_w + (J_w/r^2))\ddot{x} \quad (4)$$

The sum of forces in the  $x$ -direction can be written as (5):

$$N_x = m_c \ddot{x} + m_c \ell \ddot{\beta} \cos \beta - m_c \ell \dot{\beta}^2 \sin \beta \quad (5)$$

where  $N_x$  is the combination of forces from both wheels,  $m_c$  is the mass,  $\ell$  is the distance to the center of the mass,  $\theta$  is the angle between vertical line and the pendulum, and  $\ddot{x}$  is the robot's acceleration in the  $x$ -direction. The sum of forces perpendicular to the pendulum is simply:

$$N_y \sin \beta + N_x \cos \beta - m_c g \sin \beta - m_c \ell \ddot{\beta} = m_c \ddot{x} \cos \beta \quad (6)$$

where  $N_y$  refers to the force in the  $y$  direction, and  $g$  refers to the gravity constant. The sum of torques acting at the center of the pendulum is:

$$-N_y \ell \sin \beta - N_x \ell \cos \beta - 2T_w = J_c \ddot{\beta} \quad (7)$$

where  $J_c$  is the pendulum's moment of inertia. Assuming  $\alpha$  is sufficiently small, we have  $\sin \beta = \sin(\pi + \alpha) \approx -\alpha$ ;  $\cos \beta = \cos(\pi + \alpha) \approx -1$ ;  $\beta^2 = \alpha^2 \approx 0$ , which lead to the following approximations.

$$N_x = m_c \ddot{x} - m_c \ell \ddot{\alpha} \quad (8)$$

$$-N_y \alpha - N_x + m_c g \alpha - m_c \ell \ddot{\alpha} = -m_c \ddot{x} \quad (9)$$

$$N_y \ell \alpha + N_x \ell - 2T_w = J_c \ddot{\alpha} \quad (10)$$

By substituting the expression of  $T_w$  into (10), we will obtain.

$$N_y \ell \alpha + N_x \ell - \frac{2k_m}{R} V_{in} + \frac{2k_m k_e}{Rr} \dot{x} = J_c \ddot{\alpha} \quad (11)$$

Let  $x_1 = x$ ,  $x_2 = \dot{x}$ ,  $x_3 = \alpha$ ,  $x_4 = \dot{\alpha}$ ,  $u = V_{in}$ , and  $q = [x_1 \ x_2 \ x_3 \ x_4]^T$ , the state space representation of the TWSBR can be constructed as  $\dot{q} = Aq + Bu$ ;  $y = Cq$  with:

$$A = \begin{bmatrix} 0 & 1 & 0 & 0 \\ 0 & -\frac{2k_m k_e (J_c + m_c \ell^2 - m_c \ell r)}{\Omega R r^2} & \frac{m_c^2 \ell^2 g}{\Omega} & 0 \\ 0 & 0 & 0 & 1 \\ 0 & \frac{2k_m k_e (\Lambda r - m_c \ell)}{\Omega R r^2} & \frac{m_c g \ell \Lambda}{\Omega} & 0 \end{bmatrix}; \quad B = \begin{bmatrix} 0 \\ \frac{2k_m (J_c + m_c \ell^2 - m_c \ell r)}{\Omega R r} \\ 0 \\ \frac{2k_m (m_c \ell - \Lambda r)}{\Omega R r} \end{bmatrix} \quad (12)$$

$$C = [0 \ 0 \ 1 \ 0] \quad (13)$$

## 2.2. Control schemes for TWSBR

Figure 3 illustrates the difference between the PID control (Figure 3(a)), LQR control (Figure 3(b)) and the PID-LQR scheme (Figure 3(c)) which is proposed to overcome the limitation of each component. For the LQR control scheme, the control parameter  $K_L = [k_1 \ k_2 \ k_3 \ k_4]$  is optimized by minimizing the following cost function  $J = \int_0^\infty q^T (Q + K_L^T R K_L) q dt$  where  $Q \geq 0$  and  $R > 0$ . The optimal value of  $K_L$  can be obtained by using the formula  $K_L = R^{-1} B^T P$  where  $P$  is the solution to the Riccati equation  $A^T P + P A - P B R^{-1} B^T P + Q = 0$ . With regard to the PID control scheme, the parameters for  $K_p$ ,  $K_i$  and  $K_d$  were tuned based on the Ziegler-Nichols approach as presented in [29].

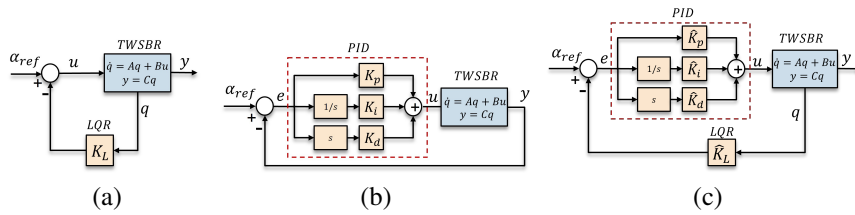


Figure 3. Illustrations on (a) the LQR and PID, (b) the proposed hybrid PID-LQR, and (c) control schemes for the TWSBR

## 2.3. Software implementation

In this work, the control schemes were designed in the LabVIEW software and deployed to the embedded NI myRIO-1900 board. The board consists of a built-in accelerometer which provides the angular acceleration from x,y, and z axes. The tilt angle from the accelerometer can be obtained as (14):

$$\alpha_{acc} = (\arctan(val(y)/val(z))) \times 180^\circ / \pi \quad (14)$$

where  $val(y)$  is the accelerometer value from the y-axis,  $val(z)$  is the accelerometer value from the z-axis, and  $T_s$  is the sampling time. However, any shock or vibration will produce sudden spikes on the tilt angle which can lead to instability of the robot. Therefore, the pitch angle of the robot was obtained through sensor fusion by combining readings from the accelerometer and a gyroscope,  $\alpha_{gyro}$ , which was externally connected to the board. A low pass filter was applied to the accelerometer to attenuate the high frequency vibration noise produced by the motors of the TWSBR. The drift from the PmodGyro's readings was minimized by applying a high pass filter. The filtered readings were then combined to obtain a more stable reading for the TWSBR. The output of the sensor fusion block is considered as the actual tilt angle of the robot, i.e.  $\alpha$ . The corresponding angular velocity,  $\dot{\alpha}$ , of the robot can be obtained by a simple mathematical calculation, i.e.  $\dot{\alpha} = (\alpha(k) - \alpha(k-1))/T_s$ .

To measure the robot's position and speed, i.e.  $x$  and  $\dot{x}$ , the angular speeds of the DC motors were firstly measured using hall-effect magnetic encoders. Since each of the hall sensors gives a resolution of 390 lines per revolution, quadruple outputs from the two hall sensors give an effective resolution of 1,560 lines per revolution. Therefore, the angular speed (in rad/s) of each motor can be calculated as follows:

$$\omega_i = (C(k) - C(k-1))/T_s \times (2\pi/1560), \quad i = R, L \quad (15)$$

where  $C(k)$  is the encoder count at iteration  $k$ , and  $\omega_R(\omega_L)$  is the angular speed of the right (left) wheel. The robot's speed and position can then be written as follows:  $\dot{x} = (\omega_R + \omega_L)r/2$  and  $x = \dot{x}T_s + x_0$  respectively where  $x_0$  is the previous position. As the controller's output will send a command that is linearly proportional to the speed, a closed-loop speed control technique from [17] is employed to ensure the actual speed of the robot follows the reference value.

### 3. RESULTS AND DISCUSSION

Based on the TWSBR model parameters in Table 1, the resulting transfer function  $G_\alpha$  is:

$$G_\alpha = \frac{39.77s}{s^3 + 66.1s^2 - 0.514s - 26.88},$$

and the  $A$  and  $B$  matrices are:

$$A = \begin{bmatrix} 0 & 1 & 0 & 0 \\ 0 & -1.1237 & 6.9748 & 0 \\ 0 & 0 & 0 & 1 \\ 0 & -255.26 & 128.9962 & 0 \end{bmatrix}; \quad B = \begin{bmatrix} 0 \\ 10.30 \\ 0 \\ 39.77 \end{bmatrix}. \quad (16)$$

Table 1. Model parameters of the robot

Notation	Definition	Value/unit
$g$	Gravitational acceleration	$9.81 \text{ m/s}^2$
$m_c$	Mass of the chassis	$0.7604 \text{ kg}$
$m_w$	Mass of each wheel	$0.048 \text{ kg}$
$J_c$	Moment of inertia of the chassis	$0.0032 \text{ kgm}^2$
$J_w$	Moment of inertia of the wheel	$0.000074 \text{ kgm}^2$
$R$	Electrical resistance of the motor	$1.6 \Omega$
$r$	Radius of the wheel	$0.034 \text{ m}$
$k_m$	Motor torque constant	$0.2182 \text{ Nm/A}$
$k_e$	Back EMF constant	$0.2182 \text{ V/(rad/s)}$
$\ell$	Half length of the chassis	$0.0 \text{ m}$

To accurately model the built robot, its linear speed is constrained within  $\pm 100 \text{ cm/s}$ . Using the LQR control design techniques in section 2.2, the values of  $Q$  and  $R$  were set to  $Q = \text{diag}(10, 10, 0, 0)$  and  $R = 1$  respectively to give the following state feedback gain  $K_L = [-3.1623 \quad 6.9428 \quad -3.9015 \quad -0.4482]$ . For the PID, the optimal values obtained were  $K_p = 300$ ;  $K_i = 5500$ ;  $K_d = 1.5$ . A filter coefficient of 10,000 was included in the PID control scheme to make the transfer function realizable. In the proposed hybrid method, some parameter tunings need to be performed to maintain the stability and improve the performance of

the closed-loop system. The optimal values obtained were  $\hat{K}_L = [-207.84 \quad 245.64 \quad -220.47 \quad -18.25]$ ,  $\hat{K}_p = 0.1$ ,  $\hat{K}_i = 0.3$  and  $\hat{K}_d = 0.7$ .

In order to evaluate the performance of the three control schemes on the TWSBR, they were tested experimentally when the robot was placed on two types of surface, i.e. rough and smooth. For each scheme, the initial tilt angle was slowly increased after each trial until the controller was no longer able to maintain the stability of the TWSBR. To provide a fair comparison, only the maximum initial tilt angle that the robot was able to self-balance and its corresponding settling time were used to evaluate the performance since the noise and disturbances entering the system were random and unmeasurable. The settling time in this case is defined as the time it takes for the tilt angle to reach within  $\pm 1^\circ$  region.

Table 2 records the numerical results while Figure 4 to Figure 6 illustrate the performance of the TWSBR with PID, LQR, and hybrid PID-LQR control schemes on both surfaces. Durations of oscillations and settling time are seen longer on smooth surface for all control schemes due to a higher probability of the robot to have wheel slips. Comparing Figure 4(a)-Figure 4(d) against Figure 5(a)-Figure 5(d), the PID is seen to be more effective at regulating the tilt angle of the robot, but it necessitates a higher linear velocity (i.e. back and forth) to sustain its equilibrium as can be observed from the trajectories of  $x_2$  in Figure 4(a), Figure 4(c), Figure 5(a), and Figure 5(c). The LQR on the other hand outperforms the PID in terms of both maximum tilt angle and settling time. Nonetheless, a significant improvement is achieved when both schemes are hybridized as can be observed from Figure 6 and the last column in Table 2 where the settling time is reduced and the maximum initial tilt angle is increased (Figure 6(a) and Figure 6(c)). Figure 6(b) and Figure 6(d) also show a considerable reduction in the amplitudes of  $x_3$  and  $x_4$ .

Table 2. Performance evaluations between PID, LQR, and hybrid LQR-PID schemes by experiments

Type of surface	Performance metric	Control scheme		
		PID	LQR	Hybrid
Rough	Maximum initial tilt angle (deg)	2.01	7.42	9.22
	Settling time (s)	2.78	2.12	2.04
Smooth	Maximum initial tilt angle (deg)	1.04	3.21	10.11
	Settling time (s)	3.02	2.13	2.12

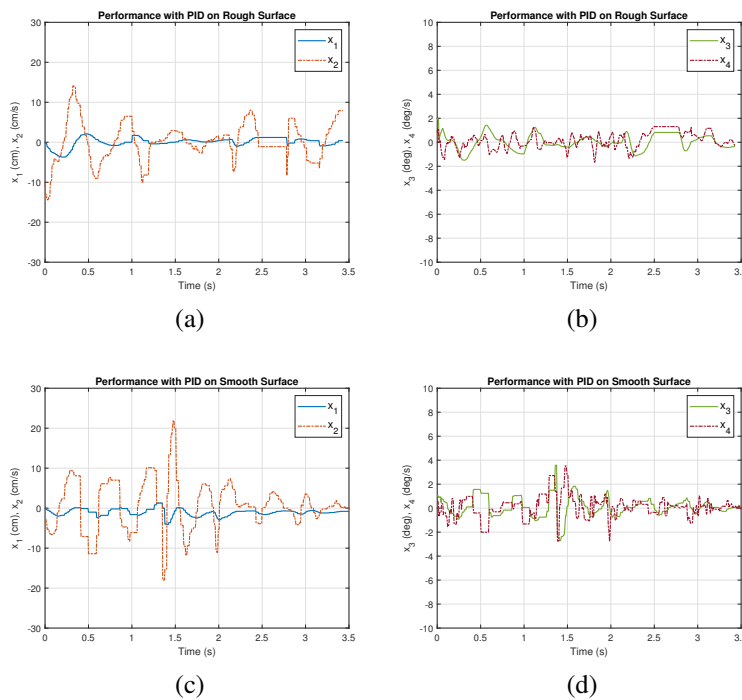


Figure 4. Performance of the TWSBR with PID control in terms of trajectories of (a)  $x_1, x_2$  on a rough surface, (b)  $x_3, x_4$  on a rough surface, (c)  $x_1, x_2$  on a smooth surface, and (d)  $x_3, x_4$  on a smooth surface

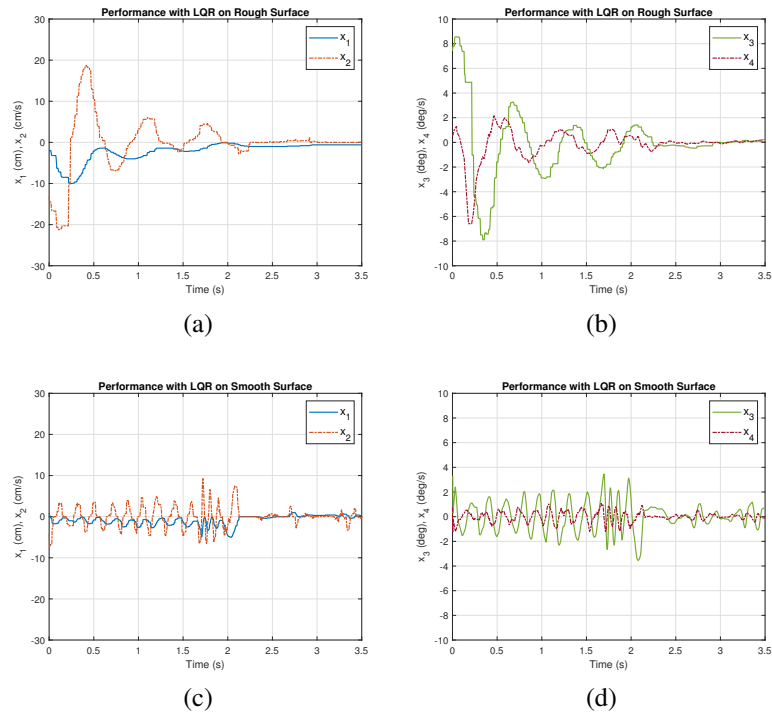


Figure 5. Performance of the TWSBR with LQR control in terms of trajectories of (a)  $x_1, x_2$  on a rough surface, (b)  $x_3, x_4$  on a rough surface, (c)  $x_1, x_2$  on a smooth surface, and (d)  $x_3, x_4$  on a smooth surface

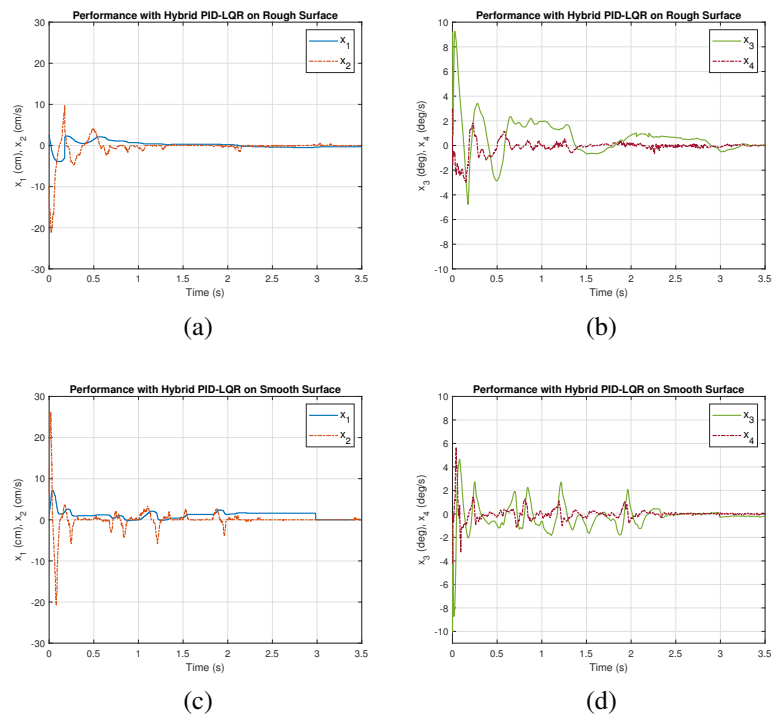


Figure 6. Performance of the TWSBR with a hybrid PID-LQR in terms of trajectories of (a)  $x_1, x_2$  on a rough surface, (b)  $x_3, x_4$  on a rough surface, (c)  $x_1, x_2$  on a smooth surface, and (d)  $x_3, x_4$  on a smooth surface

#### 4. CONCLUSION

In this study, we developed a TWSBR controlled by an embedded NI myRIO-1900 board with a model-based control scheme. Our experimental results showed that PID is more effective in regulating the robot's tilt angle in the presence of external disturbances, but it requires a higher velocity to maintain equilibrium. On the other hand, LQR outperforms PID in terms of the maximum initial tilt angle. By combining both schemes, we observed significant improvements, such as an increase in the maximum initial tilt angle and a reduction in settling time. While the experimental results presented in this study provide valuable insights into the performance of the TWSBR, future research could focus on evaluating its performance in real-world scenarios, such as navigating through complex environments or performing specific tasks. Machine learning techniques, such as reinforcement learning, could also be used to train the TWSBR to adapt to changing environmental conditions or to optimize its performance based on specific performance criteria.

#### ACKNOWLEDGEMENT

The authors would like to thank Ministry of Higher Education Malaysia for the financial support under Fundamental Research Grant Scheme with Project Code: FRGS/1/2021/TK0/USM/02/18.




#### REFERENCES

- [1] G. Fragapane, R. de Koster, F. Sgarbossa, and J. O. Strandhagen, "Planning and control of autonomous mobile robots for intralogistics: literature review and research agenda," *European Journal of Operational Research*, vol. 294, no. 2, pp. 405–426, Oct. 2021, doi: 10.1016/j.ejor.2021.01.019.
- [2] A. Loganathan and N. S. Ahmad, "A systematic review on recent advances in autonomous mobile robot navigation," *Engineering Science and Technology, an International Journal*, vol. 40, p. 101343, Apr. 2023, doi: 10.1016/j.jestech.2023.101343.
- [3] J. H. Teo, A. Loganathan, P. Goh, and N. S. Ahmad, "Autonomous mobile robot navigation via RFID signal strength sensing," *International Journal of Mechanical Engineering and Robotics Research*, vol. 9, no. 8, pp. 1140–1144, 2020, doi: 10.18178/ijmerr.9.8.1140-1144.
- [4] I. Arrouch, N. S. Ahmad, P. Goh, and J. Mohamad-Saleh, "Close proximity time-to-collision prediction for autonomous robot navigation: an exponential GPR approach," *Alexandria Engineering Journal*, vol. 61, no. 12, pp. 11171–11183, Dec. 2022, doi: 10.1016/j.aej.2022.04.041.
- [5] B. Sawatzky, I. Denison, S. Langrish, S. Richardson, K. Hiller, and B. Slobogean, "The segway personal transporter as an alternative mobility device for people with disabilities: a pilot study," *Archives of Physical Medicine and Rehabilitation*, vol. 88, no. 11, pp. 1423–1428, Nov. 2007, doi: 10.1016/j.apmr.2007.08.005.
- [6] J. Ashurst and B. Wagner, "Injuries following segway personal transporter accidents: case report and review of the literature," *Western Journal of Emergency Medicine*, vol. 16, no. 5, pp. 693–695, Sep. 2015, doi: 10.5811/westjem.2015.7.26549.
- [7] A. Pourmand, J. Liao, J. M. Pines, and M. Mazer-Amirshahi, "Segway® personal transporter-related injuries: a systematic literature review and implications for acute and emergency care," *The Journal of Emergency Medicine*, vol. 54, no. 5, pp. 630–635, May 2018, doi: 10.1016/j.jemermed.2017.12.019.
- [8] K. Hoffeld *et al.*, "Is the use of segways or e-scooters in urban areas a potential health risk? a comparison of trauma consequences," *Medicina*, vol. 58, no. 8, p. 1033, Aug. 2022, doi: 10.3390/medicina58081033.
- [9] J. A. Borja, I. Alvarado, and D. M. Peña, "Low cost two-wheels self-balancing robot for control education powered by stepper motors," *IFAC-PapersOnLine*, vol. 53, no. 2, pp. 17518–17523, 2020, doi: 10.1016/j.ifacol.2020.12.2660.
- [10] J.-H. Park and B.-K. Cho, "Development of a self-balancing robot with a control moment gyroscope," *International Journal of Advanced Robotic Systems*, vol. 15, no. 2, p. 172988141877086, Mar. 2018, doi: 10.1177/1729881418770865.
- [11] J. Iqbal, M. Ullah, S. G. Khan, B. Khelifa, and S. Čuković, "Nonlinear control systems - a brief overview of historical and recent advances," *Nonlinear Engineering*, vol. 6, no. 4, Dec. 2017, doi: 10.1515/nleng-2016-0077.
- [12] N. S. Ahmad, J. Carrasco, and W. P. Heath, "LMI searches for discrete-time Zames-Falb multipliers," in *52nd IEEE Conference on Decision and Control*, Dec. 2013, pp. 5258–5263, doi: 10.1109/CDC.2013.6760716.
- [13] N. Bekiaris-Liberis and M. Krstic, *Nonlinear control under nonconstant delays*. Philadelphia, PA: Society for Industrial and Applied Mathematics, 2013.
- [14] L. R. Silva, R. C. C. Flesch, and J. E. Normey-Rico, "Analysis of anti-windup techniques in PID control of processes with measurement noise," *IFAC-PapersOnLine*, vol. 51, no. 4, pp. 948–953, 2018, doi: 10.1016/j.ifacol.2018.06.100.
- [15] I. Jmel, H. Dimassi, S. Hadj-Said, and F. M' Sahli, "Adaptive observer-based sliding mode control for a two-wheeled self-balancing robot under terrain inclination and disturbances," *Mathematical Problems in Engineering*, vol. 2021, pp. 1–15, Jan. 2021, doi: 10.1155/2021/8853441.
- [16] Á. Odry, R. Fullér, I. J. Rudas, and P. Odry, "Fuzzy control of self-balancing robots: A control laboratory project," *Computer Applications in Engineering Education*, vol. 28, no. 3, pp. 512–535, May 2020, doi: 10.1002/cae.22219.
- [17] N. S. Ahmad, "Robust  $H_\infty$ -fuzzy logic control for enhanced tracking performance of a wheeled mobile robot in the presence of uncertain nonlinear perturbations," *Sensors*, vol. 20, no. 13, p. 3673, Jun. 2020, doi: 10.3390/s20133673.
- [18] A. Unluturk and O. Aydogdu, "Adaptive control of two-wheeled mobile balance robot capable to adapt different surfaces using a novel artificial neural network-based real-time switching dynamic controller," *International Journal of Advanced Robotic Systems*, vol. 14, no. 2, p. 172988141770089, Mar. 2017, doi: 10.1177/1729881417700893.
- [19] M. M. Rahman, S. M. H. Rashid, and M. M. Hossain, "Implementation of Q learning and deep Q network for controlling a self balancing robot model," *Robotics and Biomimetics*, vol. 5, no. 1, p. 8, Dec. 2018, doi: 10.1186/s40638-018-0091-9.




- [20] N. S. Ahmad, J. H. Teo, and P. Goh, "Gaussian process for a single-channel EEG decoder with inconspicuous stimuli and eyeblinks," *Computers, Materials & Continua*, vol. 73, no. 1, pp. 611–628, 2022, doi: 10.32604/cmc.2022.025823.
- [21] K. Chen, J. Yi, and D. Song, "Gaussian processes model-based control of underactuated balance robots," in *2019 International Conference on Robotics and Automation (ICRA)*, May 2019, pp. 4458–4464, doi: 10.1109/ICRA.2019.8794097.
- [22] J. Velagic, I. Kovac, A. Panjevic, and A. Osmanovic, "Design and control of two-wheeled and self-balancing mobile robot," in *2021 International Symposium ELMAR*, Sep. 2021, pp. 77–82, doi: 10.1109/ELMAR52657.2021.9550938.
- [23] C. V. Samak And T. V. Samak, "Design of a two-wheel self-balancing robot with the implementation of a novel state feedback for PID controller using on-board state estimation algorithm," *International Journal of Robotics Research and Development*, vol. 8, no. 2, pp. 1–10, 2018, doi: 10.24247/ijrdddec20181.
- [24] F. F. Rabbany, A. Qurthobi, and A. Suhendi, "Design of self-balancing virtual reality robot using pid control method and complementary filter," in *2021 IEEE International Conference on Industry 4.0, Artificial Intelligence, and Communications Technology (IAICT)*, Jul. 2021, pp. 15–19, doi: 10.1109/IAICT52856.2021.9532576.
- [25] M. O. Asali, F. Hadary, and B. W. Sanjaya, "Modeling, simulation, and optimal control for two-wheeled self-balancing robot," *International Journal of Electrical and Computer Engineering (IJECE)*, vol. 7, no. 4, pp. 2008–2017, Aug. 2017, doi: 10.11591/ijece.v7i4.pp2008-2017.
- [26] K. M. Goher and S. O. Fadlallah, "Bacterial foraging-optimized PID control of a two-wheeled machine with a two-directional handling mechanism," *Robotics and Biomimetics*, vol. 4, no. 1, p. 1, Dec. 2017, doi: 10.1186/s40638-017-0057-3.
- [27] J. Lin, R. Zheng, Y. Zhang, J. Feng, W. Li, and K. Luo, "CFHBA-PID algorithm: dual-loop PID balancing robot attitude control algorithm based on complementary factor and honey badger algorithm," *Sensors*, vol. 22, no. 12, p. 4492, Jun. 2022, doi: 10.3390/s22124492.
- [28] B. Kim and B. Park, "Robust control for the segway with unknown control coefficient and model uncertainties," *Sensors*, vol. 16, no. 7, p. 1000, Jun. 2016, doi: 10.3390/s16071000.
- [29] J. G. Ziegler and N. B. Nichols, "Optimum settings for automatic controllers," *Journal of Dynamic Systems, Measurement, and Control*, vol. 115, no. 2B, pp. 220–222, Jun. 1993, doi: 10.1115/1.2899060.

## BIOGRAPHIES OF AUTHORS






**Lu Bin Lau**    was born in Penang in 1998. He received the B.Eng. degree in electronic engineering from School of Electrical and Electronic Engineering, Universiti Sains Malaysia (USM) in 2022. His research interest centers around control systems and robotics. During his undergraduate studies at USM, he was actively involved in various national and international robotics competitions. He joined National Instruments as an intern in 2021, and is currently working as an electrical engineer. He can be contacted at email: laulubin@student.usm.my.



**Nur Syazreen Ahmad**    received the B.Eng. degree in electrical and electronic engineering from the University of Manchester, United Kingdom and Ph.D. degree in control systems from the same university. She is currently an associate professor at the School of Electrical and Electronic Engineering, University Sains Malaysia (USM), specializing in embedded control systems, sensor networks and mobile robotics. Her main research interest revolves around autonomous mobile robots, with a particular focus on sensing, identification, intelligent control and indoor navigation. She is a member of the IEEE Young Professional and Control System societies, and has gained a recognition as a certified LabVIEW Associate Developer by NI. She can be contacted at email: syazreen@usm.my.



**Patrick Goh**    received the B.S., M.S., and Ph.D. degrees in electrical engineering from the University of Illinois at Urbana-Champaign, Urbana, IL, USA in 2007, 2009, and 2012 respectively. Since 2012, he has been with the School of Electrical and Electronic Engineering, Universiti Sains Malaysia, where he currently specializes in the study of signal integrity for high-speed digital designs. His research interest includes the development of circuit simulation algorithms for computer-aided design tools. He was a recipient of the Raj Mittra Award in 2012 and the Harold L. Olesen Award in 2010, and has served on the technical program committee and international program committee in various IEEE and non-IEEE conferences around the world. He can be contacted at email: eep-atrick@usm.my.